Eur. Phys. J. D (2021) 75:257
https://doi.org/10.1140/epjd/s10053-021-00268-4

THE EUROPEAN PHYSICAL JOURNAL D

Regular Article - Atomic Physics

Direct observation of transitions between quantum states with energy differences below 10 neV employing a Sona unit

Ralf Engels[1,a], Markus Büscher[2,3], Paul Buske[1,8], Yuchen Gan[1], Kirill Grigoryev[1], Christoph Hanhart[1,4], Lukas Huxold[1], Chrysovalantis S. Kannis[1,5,6], Andreas Lehrach[1,5,6], Helmut Soltner[7], and Vincent Verhoeven[1]

[1] Institut für Kernphysik, Forschungszentrum Jülich, Jülich, Germany
[2] Peter-Grünberg Institut, Forschungszentrum Jülich, Jülich, Germany
[3] Institut für Laser- und Plasmaphysik, Heinrich-Heine-Universität Düsseldorf, Düsseldorf, Germany
[4] Institute for Advanced Simulation, Forschungszentrum Jülich, Jülich, Germany
[5] III. Physikalisches Institut B, RWTH Aachen University, Aachen, Germany
[6] JARA-Fame, Forschungszentrum Jülich and RWTH Aachen University, Aachen, Germany
[7] Zentralinstitut für Engineering, Elektronik und Analytik, Forschungszentrum Jülich, Jülich, Germany
[8] *Present address: Lehrstuhl für Technologie Optischer Systeme, RWTH Aachen University, Aachen, Germany*

Received 17 June 2021 / Accepted 6 September 2021 / Published online 29 September 2021

Abstract. The direct access to atomic transitions between close by quantum states employing standard spectroscopic methods is often limited by the size of the necessary radio-frequency cavities. Here we report on a new tool for fundamental spectroscopy measurements that can overcome this shortcoming. For this, a Sona transition unit was used, i.e., two opposed solenoidal coils that provide an oscillating field in the rest frame of the through-going atomic beam. In this way, we were able to control the induced photon energy down to 10 neV or $f \sim$ MHz. The tuneable parameter is the velocity of the atomic beam. For illustration of the method, we report a measurement of the hyperfine splitting energies between the substates with $F = 1$ and $m_F = -1, 0, +1$ of $2S_{1/2}$ metastable hydrogen atoms as function of a magnetic field.

1 Introduction

Nowadays, 2-photon spectroscopy [1] reaches a relative uncertainty of the spectral energies of $4.5 \cdot 10^{-15}$ and allows, for example, a precise measurement of the hyperfine-splitting energy of the $2S_{1/2}$ state of $E_{HFS} =$ 177.556860(16) MHz [2]. In parallel to the observation of transitions between energy levels with a different quantum number n, even transitions between the substates with equal n at very small energies have been measured successfully. Rabi used a Stern–Gerlach magnet as polarizer for a through-going beam to separate hydrogen atoms with different electron spins. Then, radio-frequency (RF)-induced transitions at different magnetic fields exchanged the occupation numbers between hyperfine substates, and another Stern–Gerlach magnet was used as analyzer to determine the resonance frequency as a function of the magnetic field to measure the energy difference between the substates (see Fig. 1).

Most important was the discovery of the Lamb shift by RF-induced transitions between the $2S_{1/2}$ and the $2P_{1/2}$ states of metastable hydrogen atoms passing an RF cavity, since it allows precision tests of QED. The length l of such a cavity can be estimated from the resonance frequency $f \sim 1$ GHz, which determines the wavelength λ that must be stored inside via $c = \lambda \cdot f$, to $l \sim 0.3$ m. With the skin effect of the wall material taken into account, the cavity length is slightly reduced to ~ 0.2 m. Thus, measurements of even smaller transition energies are limited by the size of such cavities that must ensure the overlap of the atomic trajectories and the radio-frequency waves. Up to now the measurement of the hyperfine-splitting energy of the $2S_{1/2}$ state by Rothery and Hessels [3] with a cavity of about 1 m length sets the limit with $E_{HFS} = 177.556785(29)$ MHz $\sim 7.34 \cdot 10^{-7}$ eV, a similar precision as in 2-photon spectroscopy.

Here we report about a new, alternative method to study directly radio frequencies in the MHz range, respectively, energy differences of $\Delta E \sim 10^{-8}$ eV and below. Instead of using an external source of radiation, we use an atomic beam with the velocity v passing through a properly chosen static magnetic field configuration (see Fig. 2) that defines due to its sinusoidal oscillation in the rest frame of the through-going particles the wavelength λ. In this case, the time of flight through the magnetic field $\Delta t = \lambda / v$ determines the

[a] e-mail: r.w.engels@fz-juelich.de (corresponding author)

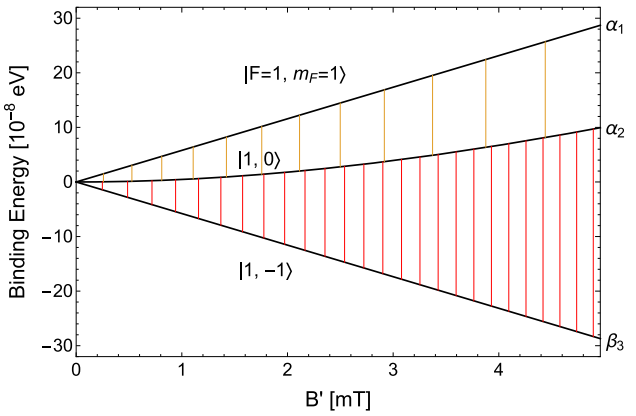

Fig. 1 The Breit–Rabi [4] diagram shows the relative binding energies of hyperfine substates as a function of an external magnetic field B'. At low magnetic fields in the Zeeman region of the metastable $2S_{1/2}$ state the energy differences between the substates with $F = 1$ and the projection $m_F = +1, 0, -1$ along an external field B' are in the order of 10^{-8} up to 10^{-7} eV. If an RF of $f = 3.54$ MHz corresponding to an energy of $1.464 \cdot 10^{-8}$ eV is applied, then (multi-)photon-induced transitions ($\alpha_2 \leftrightarrow \alpha_1$: yellow lines, $\beta_3 \leftrightarrow \alpha_2$: red lines) are only possible at magnetic fields corresponding to energy differences between these substates of $\Delta E = n \cdot h \cdot f$

induced frequency $f = 1/\Delta t = v/\lambda$. Thus, the photon energy acting on an atom can be varied by changing the velocity v of the atoms. As a first application, we present a measurement of hyperfine transitions of metastable hydrogen atoms in the $2S_{1/2}$ state, where these tiny energy differences occur naturally for easy-to-generate external magnetic fields (see Fig. 1).

In the absence of angular momentum, the total spin $J = 1/2$ of the $2S_{1/2}$ state is solely determined by the electron spin. It couples with the nuclear spin $I = 1/2$ to $F = J + I$, which can thus be either 1 or 0. For $F = 1$, three substates exist with the projection $m_F = +1, 0, -1$ onto the external magnetic field direction as quantization axis denoted as α_1, α_2 and β_3, respectively. The $F = 0, m_F = 0$ substate is called β_4. Starting with a beam of atoms in a single hyperfine substate, their interaction with photons changing the occupation numbers was studied in detail in our experiment.

2 Experimental Setup and Results

The experiment is based on a Lamb-shift polarimeter that is frequently used to measure the polarization of hydrogen and deuterium atoms [5], molecules [6] and their ions. In the 'polarizer', molecular hydrogen is ionized in an electron-impact ionizer, and the resulting protons and H_2 ions are accelerated to kinetic energies E_p between 1 and 2 keV (see Fig. 2). A Wien filter is used as velocity filter, which allows to determine the relative uncertainty of the velocity down to $\Delta v_H \sim 10^{-3}$ in the actual setup. Smaller apertures can decrease the uncertainty further, but we will limit the beam intensity and, therefore, the statistical uncertainty of the results. In parallel, the Wien filter separates H_2^+ ions from protons before they reach the cesium cell. Here, by charge exchange with cesium vapor that is obtained by heating a small amount of cesium at the bottom of the cell, metastable hydrogen atoms in all four hyperfine substates are produced. Afterward, a spinfilter quenches all metastable atoms into the ground state and allows at special resonance conditions only metastable atoms in the states α_1 or α_2 to be transmitted [7]. The next component is the Sona-transition unit [8]. It consists of two 10-cm-long solenoids providing opposing longitudinal magnetic fields with a zero crossing between the coils. If atoms in the state α_1, i.e., electron and proton spin parallel to the external magnetic field, leave the spinfilter, the inversion of the external field direction in the atomic rest frame is much faster than the Larmor precession of F. In this non-adiabatic case, the spins keep their direction along the beam axis z, whereas the magnetic field is inverted. For this to happen, the magnetic field gradient around the zero-crossing needs to fulfill the requirement [8]

$$\frac{dB_z}{dz} < \frac{8\ v_H\ m_e}{e\ r^2}, \tag{1}$$

where $v_H \approx \sqrt{2E_p/m_p}$ denotes the velocity of the hydrogen atoms, $m_p = 1.672 \cdot 10^{-27}$ kg the proton mass, $m_e = 9.109 \cdot 10^{-31}$ kg and $e = 1.602 \cdot 10^{-19}$ C the electron mass and the unit charge, respectively, and r the beam radius. This requirement can be realized by a proper choice of B, the beam energy E_p and the distance between the Sona coils. For example, a kinetic proton energy of 1.28 keV corresponds to a velocity of the hydrogen atoms $v_H = 4.93 \cdot 10^5$ m/s. For a beam radius of $r = 1$ cm, the gradient must be below $dB_z/dz < 2.2$ mT/cm or a current of 5 A in our coils, if their distance is 60 mm.

With such a setting, one expects that all atoms in state α_1 are transferred into β_3 and vice versa, i.e., m_F is changed from $+1$ into -1. This very efficient method of changing occupation numbers is also used in polarized ion sources of the Lamb-shift type [9] and at optically pumped ion sources [10].

Behind the Sona transition unit, another spinfilter is used to analyze the amount of metastable atoms in the α substates. For example, if the first spinfilter is set to transmit only atoms in the substate α_1, the Sona transition unit transfers them into β_3 and none of them is transmitted through the second spinfilter. If the Sona settings transfer some atoms back into the α_1 or α_2 substate, they can pass the second spinfilter at the corresponding resonant conditions. Afterward, these atoms reach the quenching chamber where they are quenched into the ground state by the Stark effect in a strong electric field [11]. The produced Lyman-

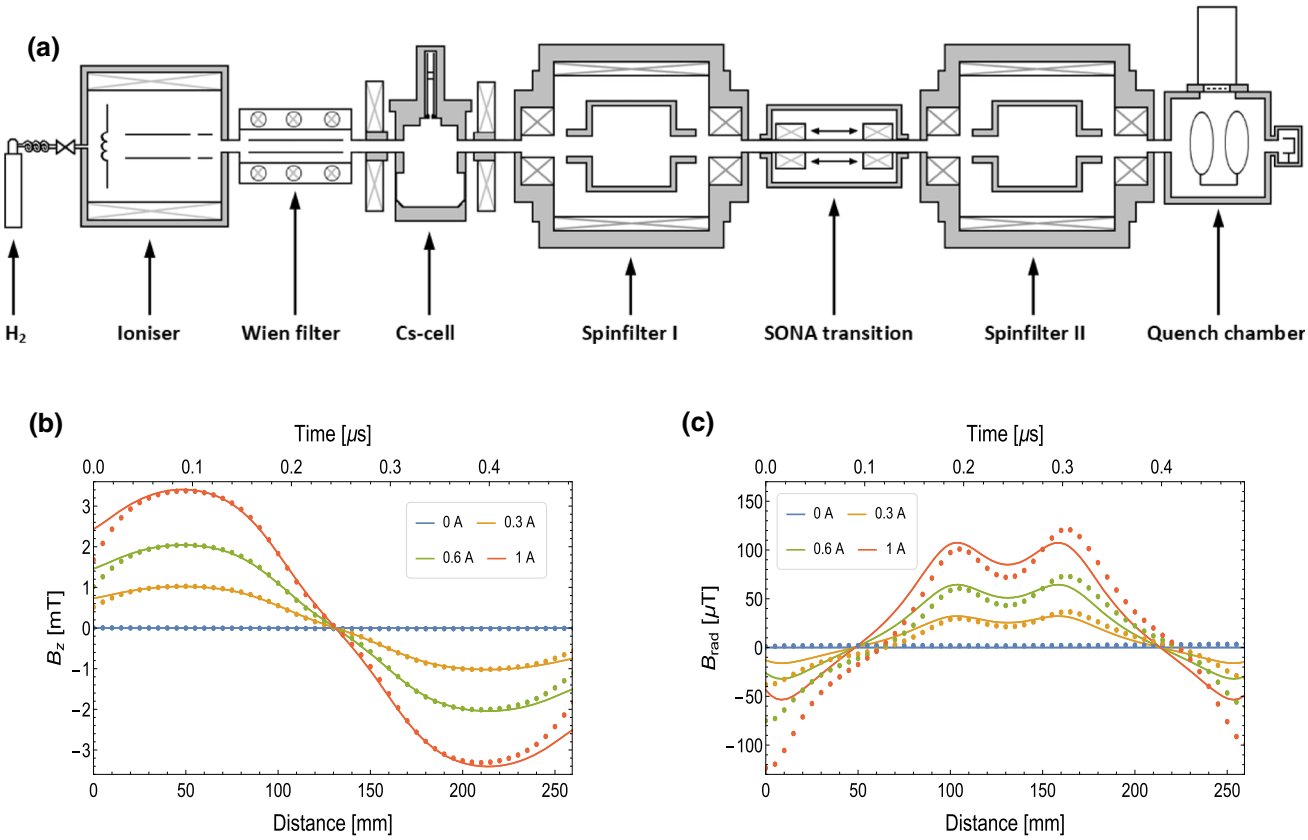

Fig. 2 Sketch of the experimental setup (a) and the calculated (line) and measured (dots) longitudinal (b) and radial (c) magnetic fields at a distance of $\rho = 3$ mm from the beam axis z for different currents in the coils of the Sona transition unit and a distance of 60 mm between the coils, which corresponds to a distance between the center of the Sona coils of 160 mm. The calibration of the maximum magnetic field B_{max} in the center of the Sona coils on the current I is $B_{max}(I) = 3.37\ \mathrm{mT/A} \cdot \mathrm{I} + 0.011\ \mathrm{mT}$. Additional shielding at both ends of the Sona transition is the reason for the deviation of measured and calculated magnetic fields

α photons are registered as a function of the current through the Sona coils. The blue lines in Figs. 3 and 4 show the measured occupation numbers for the α_1 and α_2 states. Thus, we find that for certain magnetic flux densities atoms in substates other than β_3 appear in the second spinfilter contrary to naive expectations [8].

During these first measurements, we used an electron-impact ionizer that was fed with molecular hydrogen. Thus, mainly H_2^+ molecular ions were produced and only less than 10% of all ions were protons that could pass the Wien filter for further use. This leads to a proton beam of less than 100 nA, 10^9 hydrogen atoms/s in the metastable hydrogen substate α_1 behind the first spinfilter and about 10^5 metastable atoms/s in the quenching chamber to produce a photomultiplier signal of a few mV on the oscilloscope for a typical resonance.

We note that a similar effect has been reported for a beam of hydrogen atoms in both α substates of the metastable $2S_{1/2}$ state [12–14] and even of the $1S_{1/2}$ ground state [15,16] before, but the occupation numbers of single substates have not been investigated in detail up to now.

3 Theoretical description

Since the individual atoms move on straight lines with a constant velocity through the apparatus, we can equivalently describe them in their rest frame system as experiencing a magnetic field that varies in time. The corresponding Hamilton operator describing the hyperfine substates of a hydrogen atom in an external magnetic field B is [17,18]:

$$\begin{aligned} H(t) &= \Delta E_{HFS}\ \mathbf{I}\cdot\mathbf{J} - \mu_{\mathbf{atom}}\cdot\mathbf{B}(\mathbf{t}) \\ &= \Delta E_{HFS}\ \mathbf{I}\cdot\mathbf{J} - (g_J\mu_B\mathbf{J} + g_p\mu_K\mathbf{I})\cdot\mathbf{B}(\mathbf{t}) \\ &= H_0 + V(t), \end{aligned} \tag{2}$$

where H_0 denotes the first, time-independent term. Here $g_J = -2.001$ and $g_p = 5.586$ denote the g-factors of the electron and the proton, respectively, and $\mu_K = eh/(4\pi m_p) = 1.41 \cdot 10^{-26}$ J/T is the nuclear magnetron.

The only tunable quantity is the magnetic field $\mathbf{B}(\mathbf{t})$. Its time dependence can be found directly from $\mathbf{B}(\mathbf{z})$,

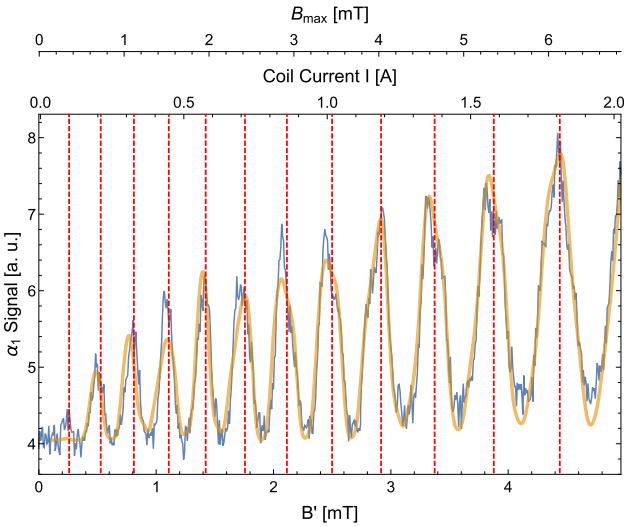

Fig. 3 Measured relative amount of metastable hydrogen atoms in the hyper-fine substate α_1 behind the Sona transition unit (blue) as a function of the effective magnetic field B' up to 5 mT, the current in the Sona coils and the corresponding max. magnetic field B_{max} at the center of the Sona coils. The small offsets between magnetic fields and the current stem from unshielded magnetic stray fields in the interaction region. In addition, the prediction of the peak centers due to the Breit–Rabi diagram (red dashed lines) and the solution of the time-dependent Schrödinger equation (yellow) for the measured magnetic field distribution B(z) and the velocity $v_H = 4.93 \cdot 10^5$ m/s ($E_{beam} = 1.28$ keV) are presented

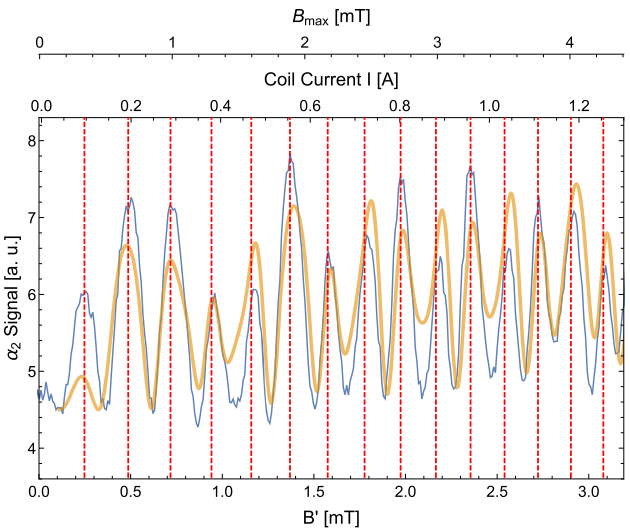

Fig. 4 The measured relative amount of metastable hydrogen atoms in the hyperfine substate α_2 behind the Sona transition unit (blue) as a function of the effective magnetic field B' up to 3.2 mT, the current in the Sona coils and the corresponding max. magnetic field B_{max} in the center of the Sona coils. Other details are found in the caption of Fig. 3

i.e., the dependence of the magnetic field along the beam direction z, due to the motion of the hydrogen atoms with velocity v_H (see Fig. 2). The radial component B_{rad} of the flux density of a solenoid at a radius ρ can be calculated from the gradient of the longitudinal field B_z via

$$B_{rad}(z,\rho) = -\frac{dB_z}{dz} \cdot \frac{\rho}{2} \tag{3}$$

employing $\boldsymbol{\nabla} \cdot \mathbf{B} = 0$ and, of course, can also be measured directly. Note that only B_{rad} can induce the observed transitions, since both terms $J_z \cdot B_z$ and $I_z \cdot B_z$ are diagonal in the basis used. Using the time-dependent Schrödinger equation and the measured $B_{rad}(z,\rho)$ with the Hamiltonian from above and expanding the solution in terms of the unperturbed wave functions (found from solving the time-independent Schrödinger equation with $V(t) = 0$),

$$\Psi(x,t) = \sum_{n=1}^{4} c_n(t) e^{-iE_n t/\hbar} |n\rangle \quad \text{with} \quad H_0|n\rangle = E_n|n\rangle$$

one finds for the expansion parameters the equation

$$i\hbar \frac{dc_k(t)}{dt} = \sum_{n=1}^{4} c_n(t) e^{\frac{-i(E_n - E_k)t}{\hbar}} \langle k|V(t)|n\rangle,$$

where the sum runs over the four basis states of the $2S$ level. The only approximation applied to derive this differential equation is that all states not belonging to the $2S$ multiplet are neglected, which is well justified given the large energy differences. Especially transitions into the $1S$ state are just perturbative and can be neglected, because the lifetime of the metastable atoms $\tau = 0.14$ s is five orders longer than the time-of-flight through the complete apparatus. For the discussion below, it is important to note that the matrix element $\langle k|V(t)|n\rangle$ only yields a contribution for quantum numbers m_F differing by ± 1.

This equation may be solved by discretizing in the time variable for the known magnetic field $B_{rad}(z,\rho)$. To find the relative occupation numbers for the different substates, one needs to integrate the resulting wave functions over the beam profile, here assumed to be of Gaussian shape with a spread $\sigma = 5$ mm. In Fig. 3 and Fig. 4, the result for the occupation number of state α_1 and α_2, respectively, is compared to the experimental data. In first order, the radial beam density profile does not affect the peak positions at the corresponding magnetic fields, but influences their amplitudes and shapes. The reason is that the RF is stable, but its power, respectively the photon density, is growing with larger ρ. Thus, assuming other radial beam distributions in the simulations, the relative intensities of the single resonances are modified, but the peak positions stay. During the experiment, the radial beam density can be manipulated by different focusing and leads to a deviation between the predictions of an ideal beam distribution and measured data like shown in the example

of Fig. 4. Nevertheless, the positions of the maxima as a function of the magnetic field are still unchanged.

It is intriguing that the locations of the peaks shown in Figs. 3 and 4 can be straightforwardly understood in a particle picture. It is the general understanding that during their passage from one Sona solenoid to the other all atoms are transferred from state α_1 into β_3. However, they can also absorb a photon to be excited into state α_2 and a second photon to reach state α_1 again. These photons are induced by the oscillation of the radial magnetic field seen by the metastable hydrogen atom in its rest frame during the flight from one Sona coil to the other. Such transitions are by far most efficient, when

$$\Delta E = n \cdot h \cdot f \tag{4}$$

holds, where n denotes an integer number. Therefore, every time the averaged magnetic field B' inside the solenoids corresponds to an energy difference between the states α_1 and α_2 that equals an integer multiple of $h \cdot f$ (see Fig. 1), this transition can appear as a peak in a scan like the one shown in Figs. 3 or 4. In other words, the transitions are induced by multi-photon absorption. The transition from α_2 into α_1 is only possible, if the state α_2 has been populated through a $\beta_3 \leftrightarrow \alpha_2$ transition before, for otherwise the transition matrix element vanishes. Since the energy differences between the states $\beta_3 \leftrightarrow \alpha_2$ and $\alpha_2 \leftrightarrow \alpha_1$ are not equal for the same magnetic field, the resonance shapes are a convolution of both transitions. The corresponding deformations of the single resonances are obvious especially in Fig. 3 for the measured data and the calculation. When the second spinfilter allows only metastable hydrogen atoms in the substate α_2 to be transmitted, the transitions from $\beta_3 \rightarrow \alpha_2$ will dominate the occupation numbers of the substate α_2 and the transitions $\alpha_2 \rightarrow \alpha_1$ are responsible for an additional deformation of the resonances (see Fig. 4).

As long as the relative velocity distribution of the metastable atoms in the beam is below ±2%, only an increased resonance width appears, whereas the peak positions stay fixed, since their locations are determined by the resonance condition. In case of even broader beam velocity profiles, the deformations are shaping the resonances more and more, and this can, since the resonances overlap, lead to a shift of the peak centers to higher or lower magnetic fields.

4 Results

The energy of the exchanged photons can be determined by different methods:

(*i*) The radial magnetic field $B_{rad}(z, \rho)$ can be transformed with the known beam velocity $v_H = dz/dt$ into $B(t, \rho)$. Thus, a Fourier analysis of the radial RF seen by the atom during its time-of-flight Δt through the Sona coils yields for $v_H = 4.93 \cdot 10^5$ m/s a first harmonic frequency of $f_0 = 1.76$ MHz and a second harmonic at $f_1 = 3.52$ MHz. Only the second harmonic corresponds to a full oscillation between the Sona coils, i.e., a photon, and can induce RF transitions between the hyperfine substates. All harmonic frequencies depend only on the velocity of the hydrogen atom v_H and the geometry of the coils and are independent of an increasing longitudinal magnetic field strength that changes the effective magnetic field strength B' and the amplitude of the oscillation, i.e., the number of photons. The corresponding wavelength of the second harmonic frequency f_1 can be calculated from the equation

$$v_H = \lambda \cdot f_1 \tag{5}$$

and is $\lambda = 140$ mm in the example of Fig. 2. Thus, the static radial magnetic field component in the laboratory system induces an oscillating radial magnetic field in the rest frame of the atom. Its frequency $f_1 = 1/\Delta t$ depends only on the velocity v_H of the beam as long as the magnetic field geometry, which defines λ, is constant. This allows one to control the induced frequency in a wide range and to observe direct transitions between quantum states with an energy difference of about 1 MHz for $v_H \sim 10^5$ m/s down to 10 kHz for beams with $v_H \sim 10^3$ m/s like in Ref. [19] as long as the Sona condition (Eq. 1) is still valid. In addition, the distance between the Sona coils can be increased to decrease the frequency even further. Here it should be mentioned that the wavelength λ of the static magnetic field oscillation is not a linear function of the distance between the Sona coils. If the coils are very close to each other the maxima of the magnetic fields in each solenoid are not in the center but shifted further from the zero-crossing in between. If the distance between the coils surpasses a limit, then the radial magnetic field at the zero-crossing will develop a second maximum like it is shown in Fig. 2c.

(*ii*) Alternatively, one can exploit the nonlinearity of the well-known binding energies of the hyperfine substates α_2 as function of the magnetic field to calibrate the frequency f_1 and the magnetic field. With an effective magnetic field B' as input, the Breit–Rabi formula can be used to calculate the energy difference between the hyperfine substates (see Fig. 1). For the measurement shown in Fig. 3, the first peak appears at a current of 0.09 A through the Sona coils that correspond to a maximum magnetic field of $B_{max} = 0.31$ mT inside the coils. For the next resonances, the differences between the corresponding magnetic fields increase for the $\alpha_2 \leftrightarrow \alpha_1$ transitions with larger n and decrease for $\beta_3 \leftrightarrow \alpha_2$. At the same time, the energy differences between the states $\Delta E = \Delta E(B') = n \cdot h \cdot f$ depend only on the integer n and the induced RF f_1, which is constant for a constant velocity of the atoms and a fixed experimental setup. In this way, a calibration for the effective magnetic field $B' = (0.723 \pm 0.003) \cdot B_{max} + (0.004 \pm 0.02)$ mT could be found with an offset at zero current due to not perfectly shielded external fields. For a scan from $I = 0$ up to 2 A in the Sona coils $n_{\max} = 12$ resonances are found for the transi-

tions between $\alpha_2 \leftrightarrow \alpha_1$ (Fig. 1 and 3) and $n_{\max} = 26$ for $\beta_3 \leftrightarrow \alpha_2$. In this way, $\Delta E_{n=1} = (1.462 \pm 0.003) \cdot 10^{-8}$ eV or $f_1 = (3.536 \pm 0.007)$ MHz was determined with the current setup, which corresponds to an absolute uncertainty of $\Delta E \sim 10^{-11}$ eV or $\Delta f \sim 10$ kHz.

5 Discussion and outlook

This new method presented here allows one to overcome limitations of radio-frequency cavities to induce transitions between quantum states with very small energy differences. It employs a bipolar static magnetic field, and a through-going beam whose velocity is the tuneable parameter. The method is in principle applicable to any kind of beam. Of course, it is necessary to polarize the beam first, e.g., with a laser, and then to analyze the induced transitions afterward. To demonstrate that the method works, in the paper it was successfully applied to induce magnetic dipole transitions between hyperfine substates of metastable hydrogen atoms. The results perfectly fit to the predictions of the Schrödinger equation. Therefore, the wavelength λ of such a transition unit can be optimized for other quantum systems, atoms or molecules, where similar energy differences should be investigated and then calibrated to a measurement with metastable hydrogen atoms of a given velocity. The wavelength λ is entirely determined by the distance of the solenoids, and the induced photon energy ΔE can be manipulated by tuning the beam velocity. Another option of such a transition unit is the measurement of further Breit–Rabi diagrams, i.e., the hyperfine splitting energy of substates with different m_F, of different atoms and molecules by ramping the magnetic field amplitudes for a given beam velocity. Further improvements, e.g., better statistics due to a new electron–cyclotron resonance (ECR) ion source for proton beams up to 20 μA, more convenient setups of the magnetic fields in the Sona transition unit and better shielding of the external fields, are expected to permit a reduction of the uncertainty by another factor 10. If the beam energy and, thus, the velocity of the protons are changed in the ionizer, ΔE and f_1 are modified too, but the fraction remains to be Planck's constant h. Thus, the statistical uncertainty can be decreased further to measure the hyperfine splitting energies of these states as function of a (small) magnetic field down to 10^{-13} eV or 100 Hz, correspondingly.

The Schrödinger equation itself has the potential to deliver an analysis that can be even more precise: If the occupation numbers of the hyperfine substates are measured like in Fig. 3, it is even possible to calculate the longitudinal magnetic field distribution $B(t)$ along the beam axis in the Sona coils from these data inversely. A Fourier expansion of the deduced radial magnetic field delivers directly the frequencies f_1 of the oscillation of the radial component B_{rad}, and therefore, the energy difference ΔE between the substates for the single resonances and the corresponding magnetic fields B'.

In principle, the type of induced transitions, e.g., magnetic or electric dipole transitions (M1 $\leftrightarrow$ E1) and the polarization of the induced photons ($\pi \leftrightarrow \sigma$ transitions), can be chosen with dedicated magnetic or even electric field configurations.

The same method works for metastable deuterium atoms as well. Here, the Sona transition unit transfers all atoms from the state $\alpha_1(F = 3/2, m_F = +3/2)$ into $\beta_4(m_F = -3/2)$ and vice versa; the spinfilter is able to separate the α substates α_1, $\alpha_2(m_F = +1/2)$, and $\alpha_3(m_F = -1/2)$.

With only minor improvements, even the described setup allows one to test the actual QED corrections [20] of the Breit–Rabi formula that are on a level of 10^{-3} up to 10^{-2} of the values for the observable transitions at our magnetic fields below 5 mT. Of course, the magnetic field amplitudes are not limited to the Zeeman region and can be expanded much further to increase the precision by observing even more oscillations.

This new type of spectroscopy is a beautiful example to describe experimental results with the tools of quantum mechanics and allows one to determine and to observe the smallest direct transitions between two quantum states. With lower beam velocities and larger distances between the coils, even smaller energy differences are directly accessible as long as the quality of the magnetic field configuration is sufficient. This precision opens the door not only to QED tests of the hyperfine splitting energies but even to a new type of parity-violation experiments with hydrogen and deuterium atoms [21] or to observe the longitudinal Stern–Gerlach effect on metastable atoms in different hyperfine substates [22].

Acknowledgements The authors wish to thank Alexander Milstein, Yurij Shestakov and Dimitri Toporkov from the Budker Institute in Novosibirsk and Alexander Belov from the Russian Academy of Science in Moscow for valuable discussions. The work has received funding from the ATHENA project of the Helmholtz Association (HGF). Lukas Huxold acknowledges support by the Deutsche Forschungsgemeinschaft within project BU 2227/1-1.

Author contributions

P.B. and Y.G. built and commissioned the different components of the Sona transition, H.S. was responsible for the design and the simulations of the magnetic field, C.H. and C.K. performed the simulations, C.K, L.H., V.V. and K.G. contributed to the measurements and analyzed data, M.B. and A.L. jointly initiated the project within ATHENA and contributed to the interpretation of the data, R.E. contributed to and analyzed the data, prepared the manuscript and supervised the work.

Funding Open Access funding enabled and organized by Projekt DEAL.

Data Availability Statement This manuscript has no associated data or the data will not be deposited.[Authors' comment: The aim of this paper was a proof-of-principle of a new method to induce transitions between nearby quantum states with tiny energy differences that were not directly observable until now. Nevertheless, with the present set up the accuracy is not competitive compared to other, indirect observations. Thus, all necessary informations on the results are given in Figs. 3 and 4. Further measurements with an improved setup and better statistics will be published later.]

References

1. A. Matveev et al., Phys. Rev. Lett. **110**, 230801 (2013). https://doi.org/10.1103/PhysRevLett.110.230801
2. N. Kolachevsky, M. Fischer, S.G. Karshenboim, T.W. Hänsch, Phys. Rev. Lett. **92**, 033003 (2004). https://doi.org/10.1103/PhysRevLett.92.033003
3. N.E. Rothery, E.A. Hessels, Phys. Rev. A **61**, 044501 (2000). https://doi.org/10.1103/PhysRevA.61.044501
4. G. Breit, I.I. Rabi, Phys. Rev. **38**, 2082 (1931). https://doi.org/10.1103/PhysRev.38.2082.2
5. R. Engels, R. Emmerich, G. Tenckhoff, H. Paetz gen. Schieck, M. Mikirtytchiants, F. Rathmann, H. Seyfarth, A. Vassiliev, Rev. Sci. Instrum. **74**, 4607 (2003). https://doi.org/10.1063/1.1619550
6. R. Engels et al., Rev. Sci. Instrum. **85**, 103505 (2014). https://doi.org/10.1063/1.4897479
7. J.L. McKibben, G.P. Lawrence, G.G. Ohlsen, Phys. Rev. Lett. **20**, 1180 (1968). https://doi.org/10.1103/PhysRevLett.20.1180
8. P.G. Sona, Energia Nucleare **14**, 295 (1967)
9. V. Bechtold, L. Friedrich, P. Ziegler, R. Aniol, G. Latzel, H. Paetz gen. Schieck, Nucl. Instrum. Methods **150**, 407 (1978). https://doi.org/10.1016/0029-554X(78)90106-4
10. A. Zelenski et al., Rev. Sci. Instrum. **73**, 888 (2002). https://doi.org/10.1063/1.1427669
11. J. Stark, Verh. Deutsch. Phys. Ges. **16**(1914)
12. R.D. Hight, R.T. Robiscoe, Phys. Rev. A **17**, 561 (1978). https://doi.org/10.1103/PhysRevA.17.561
13. R.D. Hight, R.T. Robiscoe, W.R. Thorson, Phys. Rev. A **15**, 1079 (1977). https://doi.org/10.1103/PhysRevA.15.1079
14. F. Garisto, B.C. Sanctuary, Phys. Rev. A **23**, 1234 (1981). https://doi.org/10.1103/PhysRevA.23.1234
15. A. Kponou, A. Zelenski, S. Kokhanovski, V. Zubets, A.I.P. Conf, Proc. **980**, 241 (2008). https://doi.org/10.1063/1.2888092
16. A. Zelenski, J.G. Alessi, A. Kponou, D. Raparia, in *Proc. 11th European Particle Accelerator Conf. (EPAC'08)*, Genoa, Italy, Jun. 2008, paper TUOBM03, pp. 1010–1012
17. E.P. Antishev, A.S. Belov, AIP Conf. Proc. **980**, 263 (2008). https://doi.org/10.1063/1.2888096
18. A. Milstein, Y. Shestakov, D. Toporkov, Nucl. Instrum. Methods **969**, 164046 (2020). https://doi.org/10.1016/j.nima.2020.164046
19. W.E. Lamb, R.C. Retherford, Phys. Rev. **72**, 241 (1947). https://doi.org/10.1103/PhysRev.72.241
20. D.L. Moskovkin, V.M. Shabaev, Phys. Rev. A **73**, 052506 (2006). https://doi.org/10.1103/PhysRevA.73.052506
21. T. Bergmann, M. DeKieviet, T. Gasenzer, O. Nachtmann, M.-I. Trappe, Eur. Phys. J. D **54**, 551 (2009). https://doi.org/10.1140/epjd/e2009-00179-4
22. É. Maréchal, S. Guibal, J.-L. Bossennec, M.-P. Gorza, R. Barbé, J.-C. Keller, O. Gorceixa, Eur. Phys. J. D **2**, 195 (1998). https://doi.org/10.1007/s100530050130